

Dynamics of a multicomponent vesicle in shear flow

Kai Liu, Gary R. Marple, Shuwang Li, Shravan Veerapaneni and John Lowengrub

March 21, 2017

SM.1 Nondimensionalization and Timescale analysis

Let l be the characteristic size of a vesicle (e.g., $l \sim 10^{-5}m$) and \bar{B} be the bending stiffness of the stiffer phase (e.g., $\bar{B} \sim 10^{-19}J$). Then, there are three time scales that govern the dynamics: the bending relaxation time scale $\tau_B = \eta l^3 / \bar{B}$, where η is the viscosity of the fluid, the shear time scale $\tau_S = 1/S'$, where S' is the dimensional shear rate, and the Cahn-Hilliard diffusional time scale $\tau_D = v' a'_0 / (l^2 \epsilon')$, where the primes denote the dimensional values of these parameters (a'_0 measures the line energy and ϵ' measures the excess energy due to surface gradients). The dimensional equations take the same form as Eqs. (1)-(17) in the main text, but with the nondimensional parameters replaced by corresponding ones with primes. Nondimensionalizing time by τ_B and space by l , we obtain the system given in the main text with the nondimensional parameters: $S = \tau_B / \tau_S$, $a_0 = a'_0 l / \bar{B}$, $\epsilon = \epsilon' / l$ and $v = \tau_B / (\tau_D a_0 / \epsilon)$.

In the simulations presented in the paper, we took $v = 1$, $a_0 = 100$ and $\epsilon = 0.04$, which implies that $\tau_B / \tau_D = a_0 / \epsilon = 2.5 \times 10^3$. Consequently, Cahn-Hilliard diffusion and phase separation occurs much more rapidly than motion due to bending relaxation or the applied shear ($S = \tau_B / \tau_S$ ranges from 5 to 320). This is confirmed by the analysis presented below.

We next investigate the dependence of the multicomponent vesicle dynamics upon the diffusive time scale τ_D by varying v . The results are shown in Fig. 1, where we use $v = 1/8, 1$, and 2 so that the corresponding ratios are $\tau_B / \tau_D = 3.125 \times 10^2, 2.5 \times 10^3$ and 5×10^3 , respectively. We set $\bar{\psi} = 0.3$, $\epsilon = 0.04$, $a_0 = 100$, $S = 40$, and $\Delta = 0.19$ for all three cases. As seen from the figure, the initial stages of phase separation occur at different rates, with larger v driving faster phase decomposition.

As shown in Fig. 1, the initial phase decomposition occurs more rapidly for larger v . When $t = 0.128$, the phase distributions for all the three cases are similar, despite a small shift due to tank treading. The cases with $v = 1$ and $v = 2$ are tank-treading while that with $v = 1/8$ is phase-treading. Indeed, the critical shear rate for $v = 1/8$ is $S_C = 8.5$, which is about a factor of 8 smaller than for $v = 1$ where $S_C = 72$.

SM.2 Comparison with Keller-Skalak theory

Here, we compare the tilt angle θ and the tank-treading frequency ω^t for a homogeneous membrane with the values predicted by the two-dimensional version of the Keller-Skalak theory^{1,2}. We take $L = 2.6442$, $S = 40$ and $B = 1$ and varying the shape parameter Δ . As shown in Fig. 2, when Δ is small, the numerical results agree with the 2D Keller-Skalak theory, for both tilt angle θ and the tank-treading frequency ω^t . When Δ increases so that the vesicle is more elongated, the differences between the two increase. For the tilt angle θ , the differences between them $|\theta_C - \theta_T| \sim \Delta^2$, and for the tank-treading frequency ω^t , we find $|\omega_C^t - \omega_T^t| \sim \Delta^{1/2}$, where

SM.3 The asphericity of vesicle membranes

Following Ref.³, the shape and orientation of the vesicles can be quantified by a shape parameter and inclination angle based on the gyration tensor of the vesicle membrane

$$S = \frac{1}{N} \begin{pmatrix} \sum_{i=1}^N (x_i - x_{cm})^2 & \sum_{i=1}^N (x_i - x_{cm})(y_i - y_{cm}) \\ \sum_{i=1}^N (x_i - x_{cm})(y_i - y_{cm}) & \sum_{i=1}^N (y_i - y_{cm})^2 \end{pmatrix}. \quad (\text{SM.1})$$

the subscripts C and T denote the computational results and the 2D K-S theory, respectively.

The asphericity, α_A , is defined as

$$\alpha_A = \frac{\Lambda_{max} - \Lambda_{min}}{\Lambda_{max} + \Lambda_{min}} \quad (\text{SM.2})$$

where Λ_{max} and Λ_{min} are the two eigenvalues of the gyration tensor ($\Lambda_{max} \geq \Lambda_{min}$).

In Fig. 3, we plot the time evolution of α_A and θ for selected cases of phase treading (upper and left, upper right) and tumbling (lower right). When the vesicle is phase treading the shape, as measured by α_A , and the inclination angle θ are out of phase. When the vesicle is tumbling, α_A and θ are in phase.

Further, as shown in Fig. 4, the $\theta - \alpha_A$ plane shows that during phase treading (upper left and right, lower left), the dynamics are characterized by closed loops centered around a non-zero tilt angle that is close to that for an analogous homogeneous vesicle. In contrast, when tumbling occurs (lower right), the graph is an open, periodic curve. Tank treading (not shown) would correspond to a single point in the $\theta - \alpha_A$ plane.

Note that, in some cases, there are sharp corners in the graphs in the $\theta - \alpha_A$ plane, as shown in Fig. 4 (upper left) and the close-up in Fig. 5 (upper left), when $\bar{\psi} = 0.3$, $S = 80$, and $\Delta = 0.19$. As seen in Fig. 5, the sharp corner is associated with rapid changes in α_A and θ due to the motion of the $\psi = 1$ (red) phase passing through the high curvature region of the vesicle as shown by the shape and phase distribution of the vesicle when $t = 1.86$, which is the black square in the $\theta - \alpha_A$ plot. The other vesicle morphologies shown correspond to the open circle ($t = 1.88$, $\theta = 33.99$) and triangle ($t = 1.85$, $\theta = 34.2353$).

References

- [1] S. Keller and R. Skalak, *J. Fluid Mech.*, 1982, **120**, 27.
- [2] R. Finken, A. Lamura, U. Seifert and G. Gompper, *The European Physical Journal E*, 2008, **25**, 309–321.
- [3] S. Meblinger, B. Schmidt, H. Noguchi and G. Gompper, *Phys. Rev. E*, 2009, **80**, 011901.

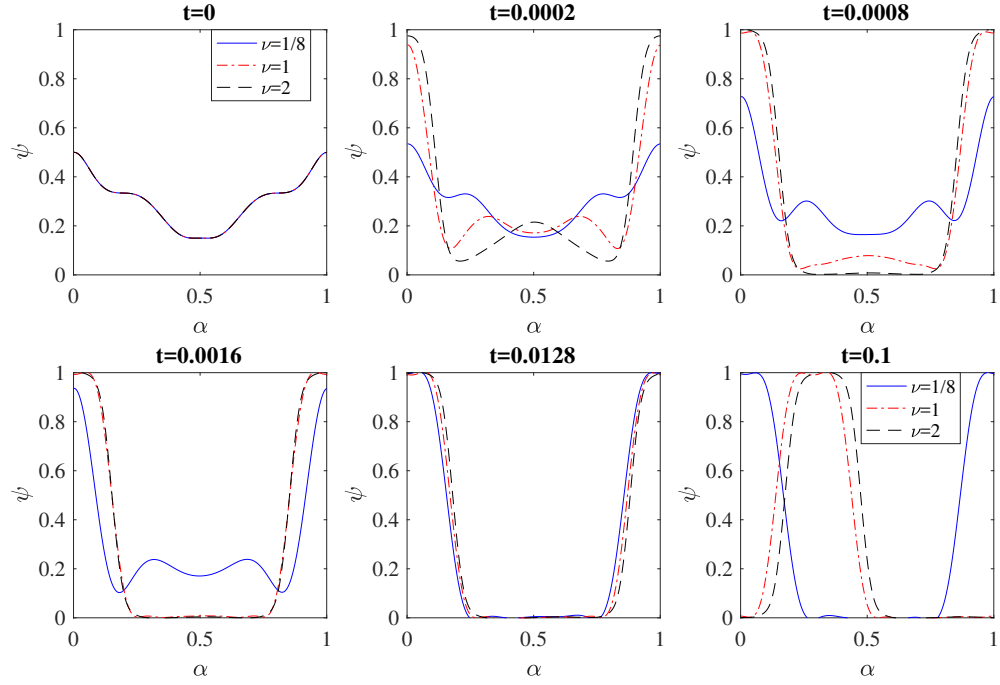


Figure 1 Multicomponent vesicle evolution with a 70 – 30 mixture of lipid phases: $\bar{\psi} = 0.3$ with fixed $\varepsilon = 0.04$, $a = 100$, $S = 40$, $\Delta = 0.19$ and varying $\nu = 1/8$ (solid), 1 (dashed-dot) and 2 (dashed). Here we plot the surface phase concentration ψ at indicated times $t = 0, 0.0002, 0.0008, 0.0016, 0.0128$, and 0.1 .

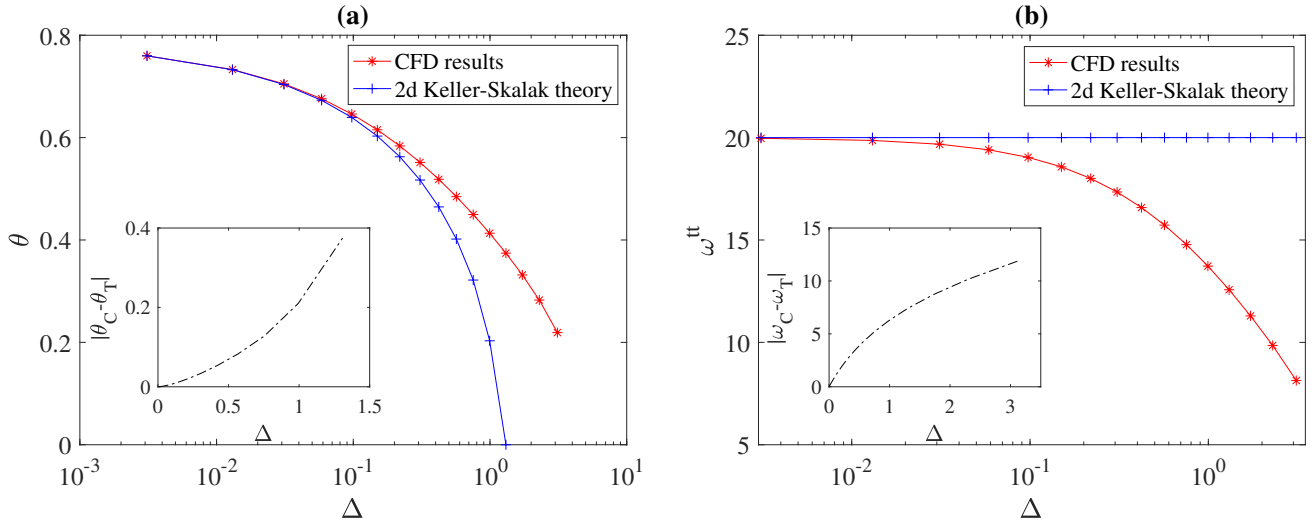


Figure 2 Comparisons of the tilt angle θ (a) and the tank-treading frequency ω_r (b) for the case of a homogeneous membrane computed with our boundary integral method with the values predicted by the two-dimensional version of the Keller-Skalak theory (see text). Here we set $L = 2.6442$, $S = 40$ and $B = 1$ and vary the excess arclength Δ .

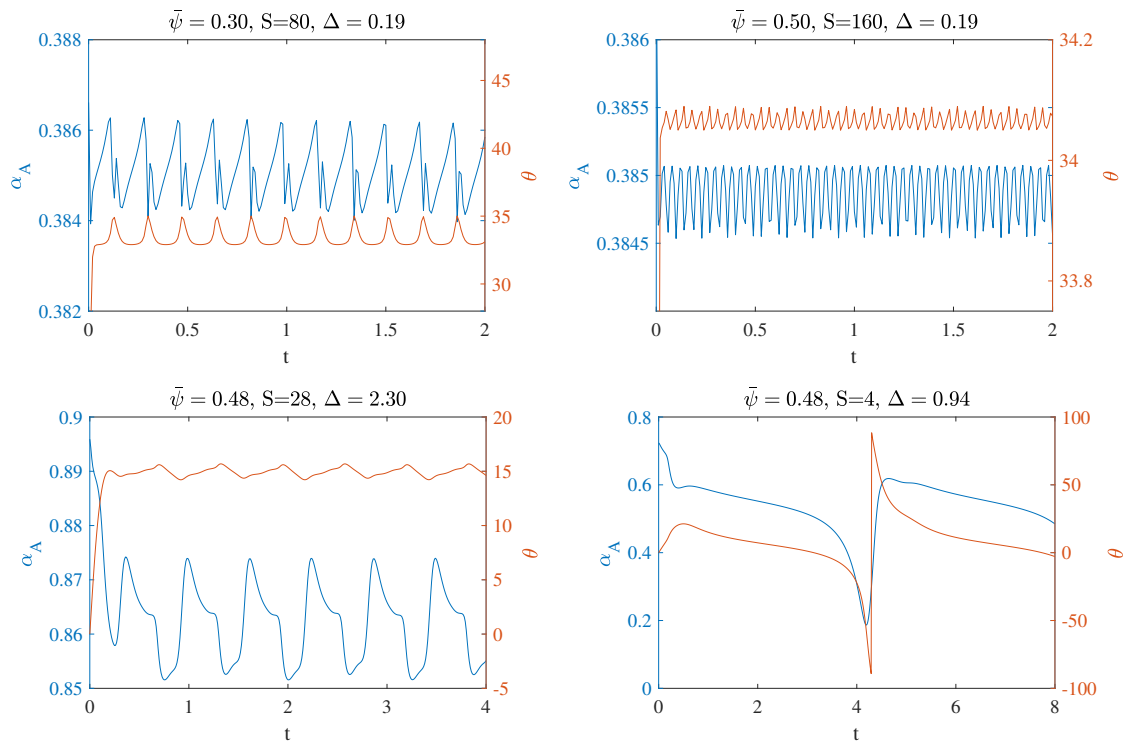


Figure 3 The dynamics of the inclination angle θ and the asphericity α_A for phase-treading (upper-left) $\bar{\psi} = 0.3$, $S = 80$, and $\Delta = 0.19$; (upper-right) $\bar{\psi} = 0.5$, $S = 160$, and $\Delta = 0.19$; (bottom-left) $\bar{\psi} = 0.48$, $S = 28$, and $\Delta = 2.30$; and tumbling (bottom-right) $\bar{\psi} = 0.48$, $S = 4$, and $\Delta = 0.94$.

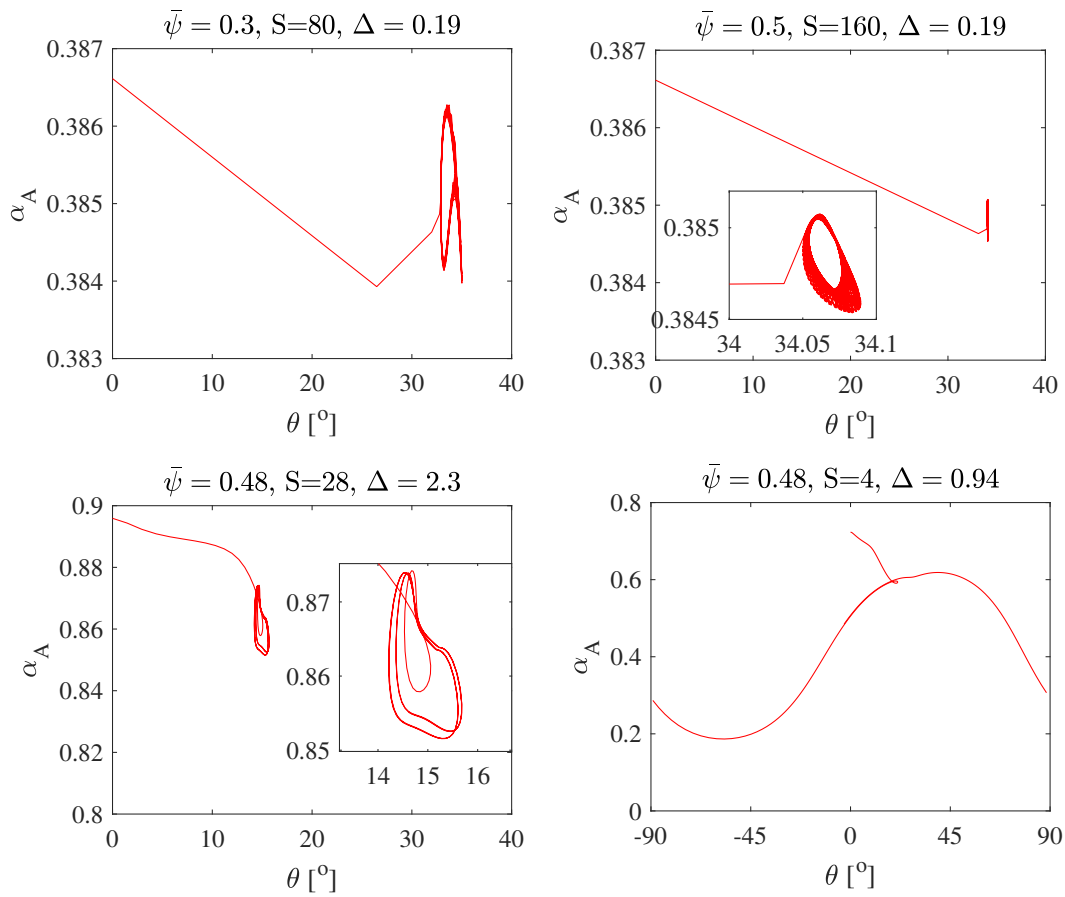


Figure 4 Trajectories in the $\theta - \alpha_A$ plane, for phase-treading (upper-left) $\bar{\psi} = 0.3, S = 80$, and $\Delta = 0.19$; (upper-right) $\bar{\psi} = 0.5, S = 160$, and $\Delta = 0.19$; (bottom-left) $\bar{\psi} = 0.48, S = 28$, and $\Delta = 2.30$; tumbling (bottom-right) $\bar{\psi} = 0.48, S = 4$, and $\Delta = 0.94$.

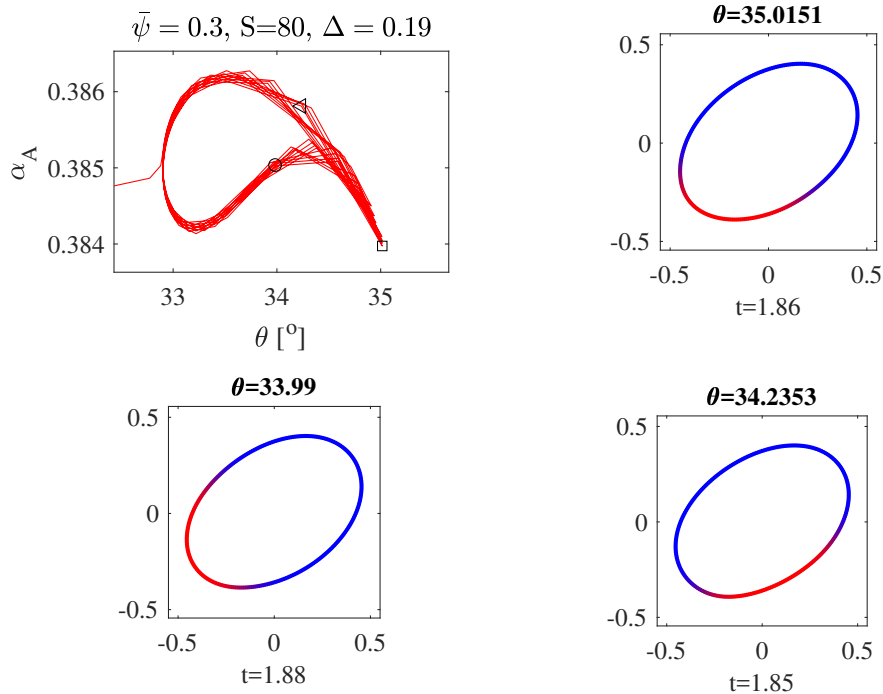


Figure 5 Trajectories in the $\theta - \alpha_A$ plane, when $\bar{\psi} = 0.3, S = 80$, and $\Delta = 0.19$. (Upper-right) picture shows the shape and phase-distribution of the vesicle at $t = 1.86$, which is denoted by the black square in the $\theta - \alpha_A$ plane.